# An extensive coronagraphic simulation applied to LBT

Vassallo, D., Carolo, E., Farinato, J., Bergomi, M., Bonavita, M., et al.

D. Vassallo, E. Carolo, J. Farinato, M. Bergomi, M. Bonavita, A. Carlotti, V. D'Orazi, D. Greggio, D. Magrin, D. Mesa, E. Pinna, A. Puglisi, M. Stangalini, C. Verinaud, V. Viotto, "An extensive coronagraphic simulation applied to LBT," Proc. SPIE 9911, Modeling, Systems Engineering, and Project Management for Astronomy VII, 99110Y (17 August 2016); doi: 10.1117/12.2234131

SPIE.

Event: SPIE Astronomical Telescopes + Instrumentation, 2016, Edinburgh, United Kingdom

# An extensive coronagraphic simulation applied to LBT

Vassallo D.[a,b,g], Carolo E.[a,g], Farinato J.[a,g], Bergomi M.[a,g], Bonavita M.[c], Carlotti A.[d], D'Orazi V.[a,g], Greggio D.[a,b,g], Magrin D.[a,g], Mesa D.[a], Pinna E.[e,g], Puglisi A.[e,g], Stangalini M.[f,g], Verinaud C.[d], and Viotto V.[a,g]

[a]INAF-OAPd, vicolo dell'Osservatorio 5, 35141 Padova, Italy
[b]University of Padova, Dept. of Physics and Astronomy, Via Marzolo 8, 35131 Padova, Italy
[c]ROE, Blackford Hill View, Edinburgh EH9 3HJ, United Kingdom
[d]IPAG, 414 Rue de la Piscine, 38400 Saint-Martin-d'Hres, Grenoble, France
[e]INAF-Arcetri, Largo Enrico Fermi 5, 50125 Firenze, Italy
[f]INAF-Roma, Via Frascati 33, 00078 Monte Porzio Catone (RM), Italy
[g]ADONI - Laboratorio Nazionale Ottiche Adattive - National Laboratory for Adaptive Optics - Italy

## ABSTRACT

In this article we report the results of a comprehensive simulation program aimed at investigating coronagraphic capabilities of SHARK-NIR, a camera selected to proceed to the final design phase at Large Binocular Telescope. For the purpose, we developed a dedicated simulation tool based on physical optics propagation. The code propagates wavefronts through SHARK optical train in an end-to-end fashion and can implement any kind of coronagraph. Detection limits can be finally computed, exploring a wide range of Strehl values and observing conditions.

**Keywords:** SHARK-NIR, Coronagraphy, Exoplanets, ADI

## 1. INTRODUCTION

SHARK[1] is an instrument proposed in the framework of LBT[2] "2014 Call for Proposals for Instrument Upgrades and New Instruments". It is composed by two channels, a visible and a near infrared one, to be installed one for each LBT telescope. The instrument will allow, in its binocular fashion, unique challenging science from exoplanet to extragalactic topics with simultaneous spectral coverage from R to H band, taking advantage of the outstanding performance of the binocular XAO LBT capability.
In this paper we present a simulation tool written in IDL language and developed to assess the coronagraphic performance of the NIR channel. The tool is aimed at the systematic investigation of a very wide parameter space, including observational strategy (number of images, integration time), atmospheric and target properties, coronagraph selection and telescope vibrations.
Section 2 describes the tool, with a brief insight into critical aspects such as coronagraphs choice and implementation of AO correction and NCPA. Section 3 introduces the data reduction pipeline, while in Section 4 we describe and analyze two case studies in order to show some possible applications of the tool.

## 2. SIMULATION TOOL

The tool generates synthetic coronagraphic images using Fresnel optical propagation. For the purpose, we chose the IDL library PROPER.[3] The routines of this library allow to propagate numerically an electric field through an optical train according to scalar theory of diffraction, in an end-to-end fashion. The propagator (i.e. numerical alghoritm) to move from one surface to the subsequent one is selected by a dedicated set of internal routines by means of analytical propagation of a gaussian pilot beam, resulting in a more accurate modeling of diffraction

Further author information: (Send correspondence to D.V.)
D.V.: E-mail: daniele.vassallo@oapd.inaf.it, Telephone: +393285771394

Modeling, Systems Engineering, and Project Management for Astronomy VII,
edited by George Z. Angeli, Philippe Dierickx, Proc. of SPIE Vol. 9911, 99110Y
 · doi: 10.1117/12.2234131

with respect to a simple Fraunhofer scheme. Finally, intrinsic limitations of physical optics propagation with respect to ray tracing do not play an important role because of the absence of refractive or highly aspherical optics in the camera, together with the excellent optical quality by design.

### 2.1 AO correction and computational time

LBT AO system FLAO (First-Light AO)[4] is a Natural Guide Star (NGS) single-conjugate system whose key strengths are the telescope adaptive secondary[5] and the pyramid wavefront sensor.[6] Since the efficiency of the AO system feeding the scientific instrument is one of the fundamental drivers of coronagraphic performance, a realistic estimate of the correction delivered by FLAO is mandatory. For the purpose, the code receives, as input phase aberration, synthetic residuals after AO correction generated with a separate code specifically modeling LBT AO system. This code has been developed in Arcetri (Florence) and has been proven to yield SR in very good agreement with on-sky measurements.
The frequency of phase screens generation is the one of the AO loop and sets the time step of simulations. The time sampling of the AO system can be adjusted according to the magnitude of the NGS. For targets brighter then $R \sim 10$, FLAO delivers wavefront correction at 1 kHz rate, meaning that a phase screen is generated every millisecond. As an example, Figure 1 shows residual rms wavefront error from simulated phase screens for a R=8 NGS and seeing of 0.4".
Following this approach, the simulation time required to generate an image of exposure $t_{exp}$ can be expressed as:

$$T = T_0 \frac{t_{exp}}{\Delta t}$$

namely a multiple of the time $T_0$ required for the numerical propagation through the whole optical train, which is primarily dependent on the size of computational matrices and on the amount of intermediate surfaces in the model of the camera. $\Delta t$ is the time step discussed before.
The code also implements an optimized parallelization scheme, which allows to reduce this time by a factor depending on the number of simultaneous threads the machine is able to handle. The final result in our simulations is $\sim$ 16 minutes per second of integration at 1 kHz rate.

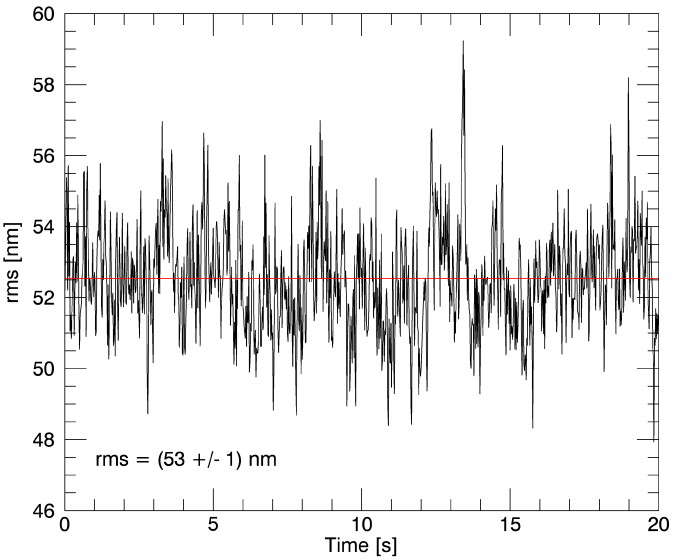


Figure 1. FLAO close-loop residual wafefront error as a function of time for a R=8 NGS and seeing of 0.4".

### 2.2 Temporal sequences and Non Common Path Aberrations

Depending on the scientific case to emulate, one may require the simulation tool to generate a single scientific frame as well as a temporal sequence. The latter is required in the case of exoplanet search, where differential imaging is mandatory if we want to attenuate the speckle floor and highlight a faint off-axis companion.
Typical total integration times in real observations are of order of several minutes up to hours: as a consequence, NCPA become an important source of noise because of their slow temporal evolution. In order to mimic this phenomenon, in simulated sequences we add to the wavefront a phase aberration which varies from frame to frame according to a specific scheme. The tool can receive as input user-specified aberration maps and can easily implement any temporal evolution scheme.
The real amount of wavefront error and the aberration temporal variation law depend on a lot of factors and are very difficult to constrain a priori. In our simulations, we adopt a simple scheme consisting of shifting a single aberration map throughout the sequence. The amount of shift has been tuned by comparing simulated sequences with real on-sky observations.

### 2.3 Coronagraphs

In addition to Lyot-class coronagraphs, the current optical design of SHARK-NIR is also compatible with three-planes techniques. This concept relies on pupil amplitude apodization and is the one adopted for the baseline coronagraphs of SPHERE[7] at VLT and GPI[8] at Gemini South. The simulation tool implements both simple circularly-symmetric apodization functions (Gaussian or Han profiles) and more complex solutions such as Shaped Pupil (SP hereafter).

#### 2.3.1 Shaped Pupil

SP masks are designed using an optimization algorithm which can account for any telescope aperture geometry.[9] Shaping the PSF, that is generating high contrast regions of a given geometry, depth and extent, is obtained with the binary apodization pattern having the maximum possible throughput. Table 1 shows some examples of these patterns for LBT pupil geometry, with the corresponding shaped PSF. All the light falling out of the high contrast region is blocked introducing a hard edge mask and a field stop. Finally, a stop is placed in the subsequent pupil plane to remove residual light diffracted at the edge of the pupil, as in the classical Lyot configuration. A gain of roughly one order of magnitude with respect to the nominal contrast of the apodizer can be reached in this way using non aberrated wavefronts.
As clearly visible, apodizers trace the support structure of LBT secondary mirror, resulting in non circularly-symmetric patterns. Therefore, because of the resulting complication in the opto-mechanical set-up, this technique can not be used when observing in field-stabilized mode (i.e. when the de-rotator is off).

## 3. DATA PROCESSING

Since the final goal of the simulation tool is to determine detection limits, physical propagation is complemented with a data processing pipeline. Here we limit ourselves to a few general considerations, since a detailed description of the pipeline is reported in Ref. 10.
In the case of a single scientific frame, the pipeline adopts as a metric the raw contrast: the tool generates an ancillary image with the same exposure time and optical set-up, but removing focal plane elements (masks, stops). The intensity in the scientific image is then normalized to the peak of this field-unobstructed PSF.
When a temporal sequence is simulated, the technique implemented in the pipeline is Angular Differential Imaging (ADI[11]): a reference PSF is obtained by median combining all images in the sequence and then is subtracted from each of them in order to remove the quasi-static structure. All image differences are then de-rotated to align the FoV and at the end a final median is performed.
An alternative approach consists in dividing the sequence into two or more subsets and performing the first step (image subtraction) separately for each of them. In this way, we obtain multiple reference PSFs, which are closer in time (and hence more correlated) to the corresponding images of the sequence with respect to a single median. The drawback is that the planet signal, if not enough field rotation has occurred in each single subset, is largely suppressed. An accurate observation plan can help mitigating this signal loss: ideally, the total duration of the observation should as long as possible, with the target close to culmination in order to maximize the total FoV

| | Pupil mask | PSF |
|---|---|---|
| IWA: 4<br>OWA: 16<br>Contrast: $10^{-5}$<br>Throughput: 30%<br>Discovery space: 360° | 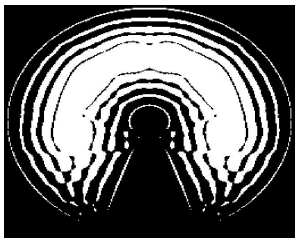 | 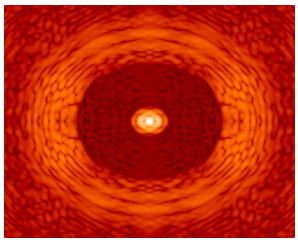 |
| IWA: 5.3<br>OWA: 12<br>Contrast: $10^{-7}$<br>Throughput: 30%<br>Discovery space: 360° | 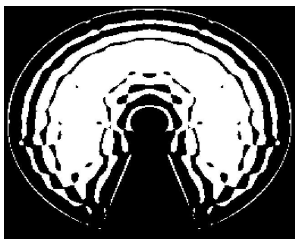 | 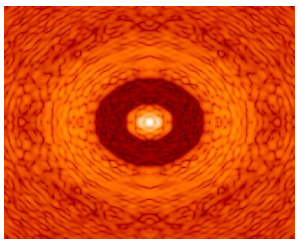 |
| IWA: 3<br>OWA: 12<br>Contrast: $10^{-6}$<br>Throughput: 30%<br>Discovery space: 240° | 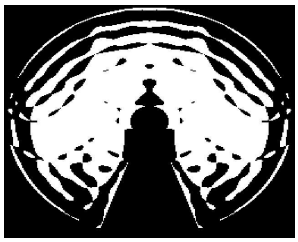 | 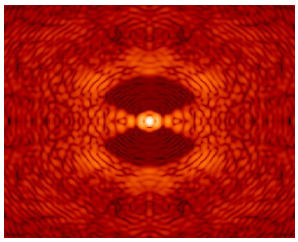 |

Table 1. Examples of Shaped Pupil masks designed for LBT, with the corresponding PSF.

rotation over the exposure.
When image differences are involved, the natural metric is the signal-to-noise ratio. The pipeline calculates the noise pixel per pixel in the final ADI-processed frame and outputs a bidimensional map. The advantage of this approach is that the spatial information is preserved, which is particularly useful in presence of non circularly-symmetric speckle patterns. Signal is computed as the peak of the field-unobstructed PSF, as in the case of raw contrast calculation. For detection limits, we assume a treshold of $5\sigma$.

## 4. APPLICATIONS: CASE STUDIES

In this section we present and discuss two case studies: an observation in pupil-stabilized mode in high SR regime and an observation in field-stabilized mode in intermediate SR regime. For both, we estimate contrast performance and compare them to the requirements of suitable science cases.

### 4.1 Pupil-Stabilized mode observation

This configuration is suitable for exoplanet search because of the possibility to apply ADI. To detect exoplanets, contrasts of order of 15 magnitudes or higher are required. We simulate a sequence of 99 frames, pointing a bright star in a night characterized by excellent seeing conditions. Concerning the coronagraph, we select the SP having an IWA of 4 $\frac{\lambda}{D}$ and 360° discovery space (see Section 2.3.1).
We introduce a phase aberration map of 8 nm rms which is assumed to be static in a single exposure, while it changes from image to image throughout the sequence in order to mimic NCPA slow evolution (see Section 2.2). Finally, a PSF movement of 3 mas rms is introduced to simulate the residual uncorrected jitter of the telescope. Table 3 summarizes the simulation set-up.

Figure 2 shows, in logarithmic scale, the non-coronagraphic PSF (i.e. with unobstructed FPs) and a coronagraphic one extracted from the simulated sequence. The latter shows the characteristic annular shape of 360° discovery space SPs (see Section 2.3.1), which is induced by the combination of occulter and field stop. Bright speckles appear near the IWA in the direction imposed for the wind in the simulation. Finally, the outer bright ring arises because of the fitting error of the AO system (the control radius is smaller than the OWA of the coronagraph).

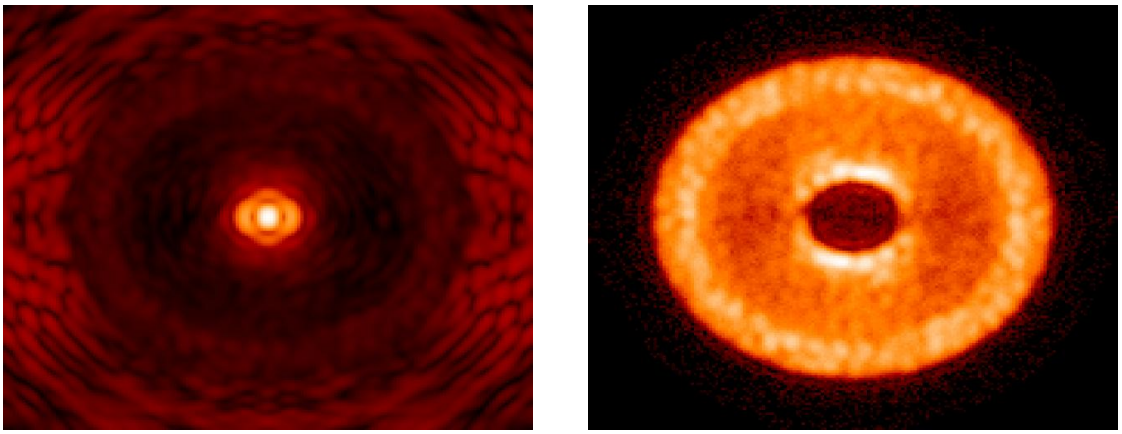

(a) (b)

Figure 2. Simulated high SR PSFs with the SP coronagraph, without (a) and with (b) occulter+field stop in the focal plane after the apodizer.

| Observation | | Target star | | Atmosphere | | Telescope | |
|---|---|---|---|---|---|---|---|
| Mode | Pupil-stabilized | R | 5 | seeing ["] | 0.4 | NCPA [nm rms] | 8 |
| Coronagraph | Shaped Pupil | H | 5 | wind speed [m/s] | 15 | jitter [mas rms] | 3 |
| Number of images | 99 | | | | | | |
| DIT [s] | 1.0 | | | | | | |
| Wavelength [$\mu m$] | 1.6 | | | | | | |
| SR | 95% | | | | | | |

Table 2. Parameters used for the simulation of a pupil-stabilized mode observation in high SR regime.

We perform ADI dividing the sequence in ten sub-groups (see Section 3). To account for off-axis sources self-subtraction, a signal loss of 10% is assumed. Figure 3 shows the final residual image. As natural, residuals trace the speckle intensity distribution in raw images of the sequence. The brightest residual feature, marked with a white circle, has a contrast of $\sim 12.4$ mag.
Detection limit as a function of angular separation is shown in Figure 4. The profile in the direction perpendicular to the wind reveals a gain of $\sim 0.5$ mag up to an angular separation of 450 mas with respect to the azimuthally averaged one.

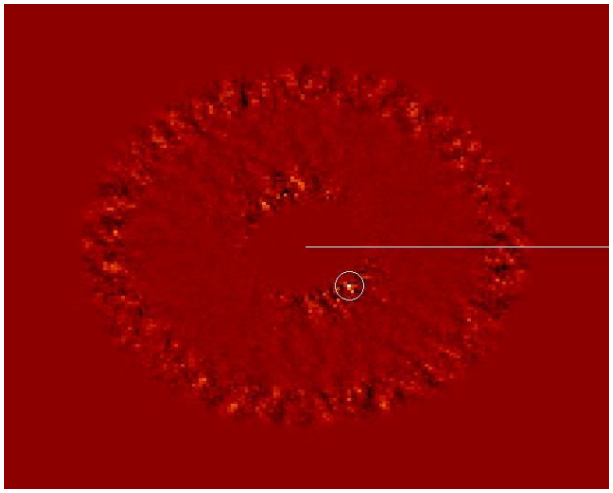

Figure 3. Final ADI-processed image. The white circle highlights the brightest speckle.

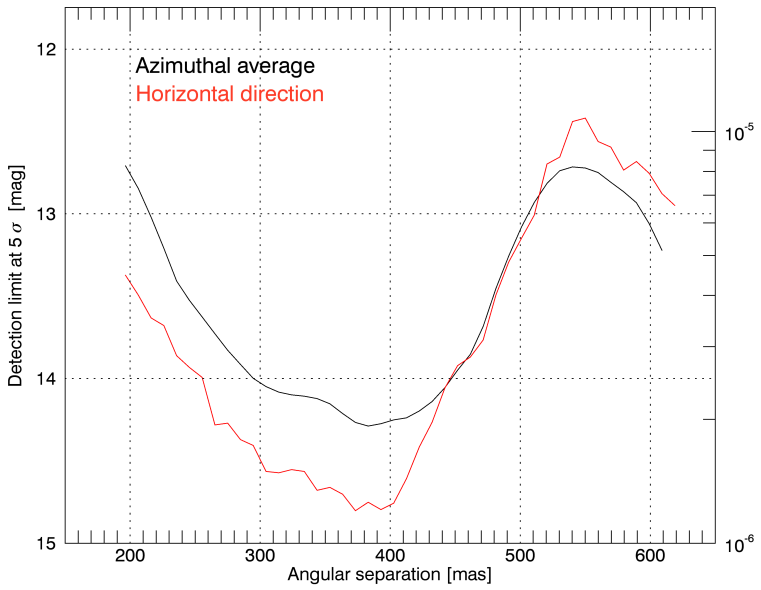


Figure 4. One-dimensional $5\sigma$ detection curves generated via azimuthal average (black line) and considering only pixels along the direction marked with the white line in the residuals map (red line).

### 4.2 Field-Stabilized mode observation

Near-IR observations aimed at probing dust grain physics in proto-planetary disks or investing stellar jets structures require field-stabilized observations. This is obtained in SHARK-NIR by mechanically de-rotating the instrument. Typical contrasts in this cases range between 8 and 12 magnitudes, therefore extreme SR is not mandatory. Here we acquire a single coronagraphic image and, since pupil apodization can not be used in this observing mode, we decide for a Gaussian Lyot coronagraph with 4 $\frac{\lambda}{D}$ IWA. Finally, we assume a $R = 10$ target and two different seeing conditions (0.4" and 0.8").
Concerning NCPA, we introduce a phase aberration of 30 nm rms, which we can reasonably assume to be static throughout the exposure.

| Observation | | Target star | | Atmosphere | | Telescope | |
|---|---|---|---|---|---|---|---|
| Mode | Field-stabilized | R | 10 | seeing ["] | 0.4/0.8 | NCPA [nm rms] | 30 |
| Coronagraph | Gaussian Lyot | H | 10 | wind speed [m/s] | 15 | jitter [mas rms] | 3 |
| Number of images | 1 | | | | | | |
| DIT [s] | 5.0 | | | | | | |
| Wavelength [$\mu m$] | 1.6 | | | | | | |
| SR | $70\% \div 85\%$ | | | | | | |

Table 3. Parameters used for the simulation of a field-stabilized mode observation in intermediate SR regime.

Figure 5 shows the coronagraphic image. Againg, bright speckles appear at small angular separations in the direction imposed for the wind. Figure 6 and 7 show raw contrast radial profiles with the two different seeing values.

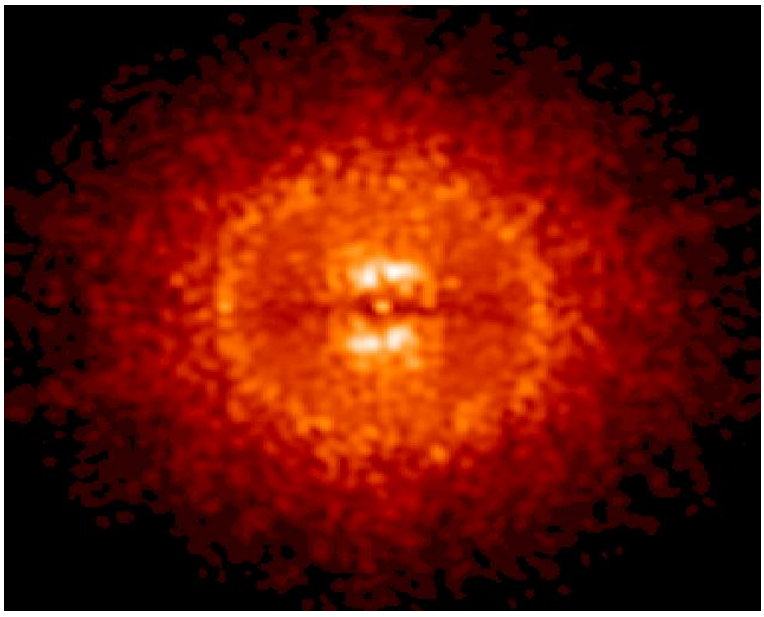

Figure 5. Simulated PSF with the Gaussian Lyot coronagraph. Seeing is 0.8".

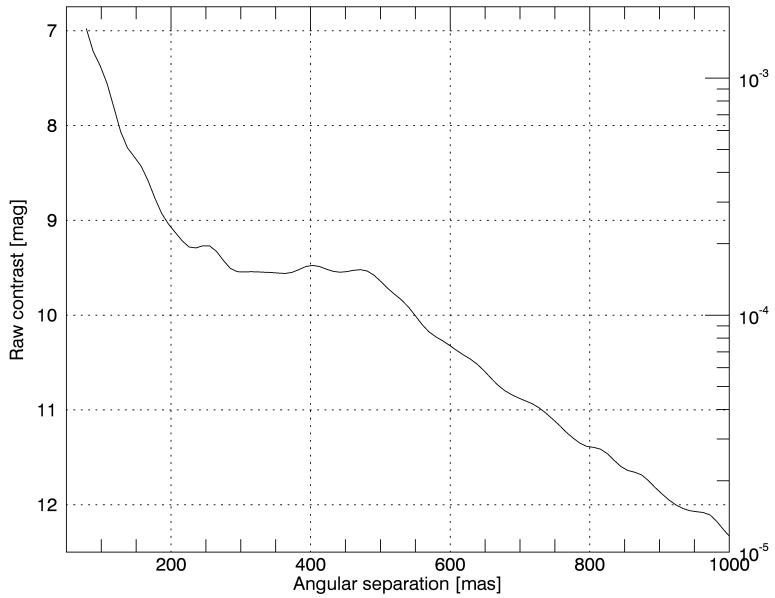


Figure 6. Raw contrast radial profile with Gaussian Lyot coronagraph. R magnitude of the target is 10 and seeing is 0.4".

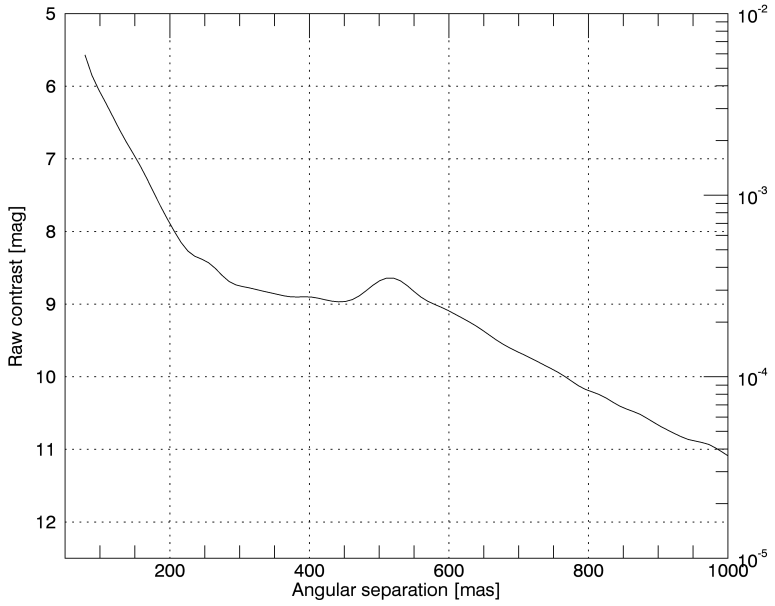


Figure 7. Raw contrast radial profile with Gaussian Lyot coronagraph. R magnitude of the target is 10 and seeing is 0.8".

## 5. CONCLUSIONS

In this paper we described a simulation tool developed to investigate coronagraphic performance of SHARK-NIR, a camera proposed as a second generation instrument for LBT. The tool implements different coronographic techniques and makes use of closed-loop AO-corrected wavefronts in a wide range of operative conditions.
We performed two test simulations, with the purpose of showing some possible applications of the tool and, at the same time, providing an estimate of contrasts achievable with the camera.
In high Strehl regime, the condition suitable for exoplanet search, observing in pupil-stabilized mode with a SP coronograph and performing ADI we can reach contrasts between $14 - 15$ magnitudes inside the control radius of the AO system.
In intermediate Strehl regime, suitable for example for direct imaging of disks and jets, with a Gaussian Lyot coronograph in field-stabilized mode we can reach a maximum contrast inside the control radius of 9.5 magnitudes with excellent seeing (0.4"), with a $\sim 0.5$ magnitude loss going to 0.8".
In both cases, estimated performance is comparable with scientific requirements.

## REFERENCES


[1] Farinato, J., Baffa, C., Baruffolo, A., Bergomi, M., Carbonaro, L., Carlotti, A., Centrone, M., Codona, J., Dima, M., Esposito, S., Fantinel, D., Farisato, G., Gaessler, W., Giallongo, E., Greggio, D., Hinz, P., Lisi, F., Magrin, D., Marafatto, L., Pedichini, F., Pinna, E., Puglisi, A., Ragazzoni, R., Salasnich, B., Stangalini, M., Verinaud, C., and Viotto, V., "The NIR arm of SHARK: System for coronagraphy with High-order Adaptive optics from R to K bands," *International Journal of Astrobiology* **14**, 365 (Jul. 2015).

[2] Hill, J. M., Green, R. F., Ashby, D. S., Brynnel, J. G., Cushing, N. J., Little, J. K., Slagle, J. H., and Wagner, R. M., "The Large Binocular Telescope," *Society of Photo-Optical Instrumentation Engineers (SPIE) Conference Series* **8444** (Sept. 2012).

[3] Krist, J. E., "PROPER: an optical propagation library for IDL," *Society of Photo-Optical Instrumentation Engineers (SPIE) Conference Series* **6675** (Sept. 2007).

[4] Esposito, S., Riccardi, A., and Fini, L., "LBT AO on-sky results," *Second International Conference on Adaptive Optics for Extremely Large Telescopes* (2011).

[5] Riccardi, A., Xompero, M., Briguglio, R., Quiros-Pacheco, F., Busoni, L., Fini, L., Puglisi, A., Esposito, S., Arcidiacono, C., Pinna, E., Ranfagni, P., Salinari, P., Brusa, G., Demers, R., Biasi, R., and Gallieni, D., "The adaptive secondary mirror for the Large Binocular Telescope: optical acceptance test and preliminary on-sky commissioning results," *Society of Photo-Optical Instrumentation Engineers (SPIE) Conference Series* **7736** (Jul. 2010).

[6] Ragazzoni, R. and Farinato, J., "Sensitivity of a pyramidic Wave Front sensor in closed loop Adaptive Optics," *Astronomy and Astrophysics* **350**, L23–L26 (Oct. 1999).

[7] Guerri, G., Daban, J. B., Robbe-Dubois, S., Douet, R., Abe, L., Baudrand, J., Carbillet, M., Boccaletti, A., Bendjoya, P., Gouvret, C., and Vakili, F., "Apodized lyot coronagraph for SPHERE/VLT: II. laboratory tests and performance," *Experimental Astronomy* **30**, 59 (May 2011).

[8] Sivaramakrishnan, A., Soummer, R., Oppenheimer, B. R., Carr, G. L., Mey, J. L., Brenner, D., Mandeville, C. W., Zimmerman, N., Macintosh, B. A., Graham, J. R., Saddlemyer, L., Bauman, B., Carlotti, A., Pueyo, L., Tuthill, P. G., Dorrer, C., Roberts, R., and Greenbaum, A., "Gemini planet imager coronagraph testbed results," *Society of Photo-Optical Instrumentation Engineers (SPIE) Conference Series* **7735** (Jul. 2010).

[9] Carlotti, A., Vanderbei, R., and Kasdin, N. J., "Optimal pupil apodizations of arbitrary apertures for high-contrast imaging," *Optics Express* **19**, 26796 (2011).

[10] Carolo, E., Vassallo, D., Farinato, J., Bergomi, M., Bonavita, M., Carlotti, A., D'orazi, V., Greggio, D., Magrin, D., Mesa, D., Pinna, E., Puglisi, A., Stangalini, M., Verinaud, C., and Viotto, V., "A comparison between different coronagraphic data reduction techniques," *Proc. SPIE* **in press** (2016).

[11] Marois, C., Lafreniere, D., Doyon, R., Macintosh, B., and Nadeau, D., "Angular differential imaging: A powerful high-contrast imaging technique," *The Astrophysical Journal* **641**, 556 (2006).